

Research Articles: Behavioral/Cognitive

Hand-selective visual regions represent how to grasp 3D tools: brain decoding during real actions

<https://doi.org/10.1523/JNEUROSCI.0083-21.2021>

Cite as: J. Neurosci 2021; 10.1523/JNEUROSCI.0083-21.2021

Received: 11 January 2021

Revised: 23 March 2021

Accepted: 29 March 2021

This Early Release article has been peer-reviewed and accepted, but has not been through the composition and copyediting processes. The final version may differ slightly in style or formatting and will contain links to any extended data.

Alerts: Sign up at www.jneurosci.org/alerts to receive customized email alerts when the fully formatted version of this article is published.

Copyright © 2021 Knights et al.

This is an open-access article distributed under the terms of the Creative Commons Attribution 4.0 International license, which permits unrestricted use, distribution and reproduction in any medium provided that the original work is properly attributed.

1 **Title**

2 Hand-selective visual regions represent how to grasp 3D tools: brain decoding during real
3 actions

4

5 **Abbreviated title**

6 Decoding tool grasping in hand-selective cortex

7

8 **Authors & Affiliations**

9 Ethan Knights^a, Courtney Mansfield^b, Diana Tonin^b, Janak Saada^c, Fraser W. Smith^b, &
10 Stéphanie Rossit^b

11 ^a Medical Research Council Cognition & Brain Sciences Unit, University of Cambridge,
12 Cambridge, CB2 7EF, UK

13 ^b School of Psychology, University of East Anglia, Norwich, NR4 7TJ, UK

14 ^c Department of Radiology, Norfolk and Norwich University Hospitals NHS Foundation Trust,
15 Norwich, NR4 7UY, UK

16

17 **Corresponding author**

18 Stephanie Rossit; s.rossit@uea.ac.uk

19

20 **Page/Word Counts**

21 Number of pages = 33 pages

22 Figures = 4

23 Tables = 1

24 Number of words for Abstract = 250 words

25 Number of words for Introduction = 643 words

26 Number of words for Discussion = 1500 words

27

28 **Conflict of interest statement**

29 The authors declare no competing financial interests.

30

31 **Acknowledgements**

32 We thank Jenna Green, Richard Greenwood, Holly Weaver, Iwona Szymura and Emmeline
33 Mottram for support in data collection, Derek Quinlan for building the real action set-up, Stefania
34 Bracci for sharing the visual localizer stimuli and Annie Warman for comments on draft
35 manuscript. This work was funded by grant (184/14) from the BIAL Foundation awarded to S.
36 Rossit & F.W. Smith.

37 **Abstract**

38 Most neuroimaging experiments that investigate how tools and their actions are represented in
39 the brain use visual paradigms where tools or hands are displayed as 2D images and no real
40 movements are performed. These studies discovered selective visual responses in occipito-
41 temporal and parietal cortices for viewing pictures of hands or tools, which are assumed to reflect
42 action processing, but this has rarely been directly investigated. Here, we examined the
43 responses of independently visually defined category-selective brain areas when participants
44 grasped 3D tools (N=20; 9 females). Using real action fMRI and multi-voxel pattern analysis, we
45 found that grasp typicality representations (i.e., whether a tool is grasped appropriately for use)
46 were decodable from hand-selective areas in occipito-temporal and parietal cortices, but not from
47 tool-, object-, or body-selective areas, even if partially overlapping. Importantly, these effects
48 were exclusive for actions with tools, but not for biomechanically matched actions with control
49 non-tools. In addition, grasp typicality decoding was significantly higher in hand than tool-
50 selective parietal regions. Notably, grasp typicality representations were automatically evoked
51 even when there was no requirement for tool use and participants were naïve to object category
52 (tool vs non-tools). Finding a specificity for typical tool grasping in hand-, rather than tool-,
53 selective regions challenges the long-standing assumption that activation for viewing tool images
54 reflects sensorimotor processing linked to tool manipulation. Instead, our results show that
55 typicality representations for tool grasping are automatically evoked in visual regions specialised
56 for representing the human hand, the brain's primary *tool* for interacting with the world.

57

58 **Significance Statement**

59 The unique ability of humans to manufacture and use tools is unsurpassed across the animal
60 kingdom, with tool use considered a defining feature of our species. Most neuroscientific studies
61 that investigate the brain mechanisms that support tool use, record brain activity while people
62 simply view images of tools or hands and not when people perform actual hand movements with
63 tools. Here we show that specific areas of the human visual system that preferentially process
64 hands automatically encode how to appropriately grasp 3D tools, even when no actual tool use is
65 required. These findings suggest that visual areas optimized for processing hands represent

- 66 fundamental aspects of tool grasping in humans, such as which side they should be grasped for
- 67 correct manipulation.

68 **INTRODUCTION**

69 The emergence of handheld tools (e.g., a spoon) marks the beginning of a major discontinuity
70 between humans and our closest primate relatives (Ambrose, 2001). Unlike other manipulable
71 objects (e.g., books), tools are tightly associated with predictable motor routines (Johnson-Frey,
72 2004). A highly replicable functional imaging finding is that simply viewing tool pictures activates
73 sensorimotor brain areas (Lewis, 2006), but what drives this functional selectivity? One popular
74 idea is that this visually-evoked activation reflects the automatic extraction of information about
75 the actions tools afford, like the hand movements required for their use (e.g., Martin et al., 1996;
76 Fang & He, 2005). Similarly, tool-selective visual responses in Supramarginal (SMG) or posterior
77 Middle Temporal Gyri (pMTG) are often interpreted as indirect evidence that these regions are
78 involved in real tool manipulation (e.g., Buxbaum et al., 2006; Bach et al., 2010). Nevertheless,
79 we would never grasp a picture of a tool and, more importantly, finding spatially overlapping
80 activation between two tasks does not directly imply that the same neural representations are
81 being triggered (Dinstein et al., 2008; Martin, 2016). In fact, intraparietal activation for viewing
82 tool pictures vs grasping shows poor correspondence (Valyear et al., 2007; Gallivan et al., 2013),
83 questioning the long-standing assumption that visual tool-selectivity represents sensorimotor
84 aspects of manipulation.

85 Curiously, the visual regions activated by viewing pictures of hands in the left Intraparietal
86 Sulcus (IPS-Hand) and Lateral Occipital Temporal Cortex (LOT-Hand) overlap with their
87 respective tool-selective areas (IPS-Tool; LOT-Tool; Bracci et al., 2012; 2013; 2016). Stimulus
88 features often described to drive the organisation of category-selective areas, like form (Coggan
89 et al., 2016), animacy (Konkle & Caramazza, 2013) or manipulability (Mahon et al., 2007) poorly
90 explain this shared topography because hands and tools differ on these dimensions. Instead,
91 their overlap is suggested to result from a joint representation of high-level action information
92 related to skilful object manipulation (Bracci et al., 2012; 2016; Striem-Amit et al., 2017), perhaps
93 coding the function of hand configurations (Perini et al., 2014; Bracci et al., 2018). Arguably, the
94 only way to directly test whether tool- or hand-selective visual areas carry information about tool
95 actions is to examine their responses during real 3D tool manipulation. Yet, very few fMRI
96 studies involve real tool manipulation (e.g., Gallivan, et al., 2009; Valyear et al., 2012; Brandi et

97 al., 2014; Styrkowiec et al., 2019). To date, only Gallivan et al. (2013) investigated real tool
98 manipulation in visually defined tool-selective regions and showed that IPS-/LOTc-Tool are
99 indeed sensitive to coarsely different biomechanical actions (reaching vs grasping) with a pair of
100 tongs. However, it remains unknown whether hand-selective visual areas represent properties of
101 real hand movements with 3D tools, like the way they are typically grasped for subsequent use.

102 Here, an fMRI experiment involving real hand actions (Fig. 1) tested if visually defined
103 hand- and tool-selective areas represented how to typically grasp 3D tools. Specifically,
104 participants grasped 3D-printed tools in ways either consistent with their use (typical: by their
105 handle) or not (atypical: by their functional-end; e.g., knife blade). As a control, non-tool bars
106 (matched with the tools for elongation, width and depth; adapted from Brandi et al., 2014) were
107 also grasped on their right or left sides to match as much as possible any biomechanical
108 differences between typical and atypical actions. Multivoxel Pattern Analysis (MVPA) was used
109 to assess whether different tool grasps (typical vs atypical) and non-tool grasps (right vs left),
110 could be decoded from fMRI activity patterns within independent visually defined Regions of
111 Interest (ROIs). Greater-than-chance decoding accuracy of typical vs atypical actions for tools,
112 but not control non-tools, was interpreted as evidence that an area contains high-level typicality
113 representations about how a tool should be grasped correctly for use (i.e., by its handle). This
114 pattern of findings was expected only for the tool- and hand-selective areas since these are
115 thought to support tool manipulation (e.g., Mahon & Caramazza, 2009; Striem-Amit et al., 2017).

116

117

118

Please insert Figure 1 here

119

120

121 **Materials and Methods**

122 **Participants.** Twenty healthy participants (11 males) completed the real action fMRI experiment
123 followed by a visual localizer experiment on a separate day. Data from one participant (male)
124 was excluded from statistical analysis due to excessive head movements during the real action
125 experiment (i.e., translation and rotation exceeded 1.5mm and 1.5° rotation) leaving a total

126 sample of 19 participants (mean age = 23 years \pm 4.2 years; age range = 18 - 34). All
127 participants had normal or corrected-to-normal vision, no history of neurological or psychiatric
128 disorders, were right-handed (Oldfield, 1971) and gave written consent in line with procedures
129 approved by the School of Psychology ethics committee at the University of East Anglia.

130

131 **Real action 3D stimuli.** Tool and non-tool object categories were designed (Autodesk Inc.) and
132 3D-printed (Objet30 Desktop) in VeroWhite material (Statasys): three common kitchen tools
133 (knife, spoon and pizzacutter) and three non-tool control bars (see Fig.1A). Objects were secured
134 to slots placed onto black pedestals used for stimulus presentation. Tools had identical handles
135 (length x width x depth dimensions of 11.6cm x 1.9cm x 1.1cm) with different functional-ends
136 attached (knife = 10.1cm x 1.9cm x 0.2cm; spoon = 10.1cm x 4.1cm x 0.7cm; pizzacutter =
137 10.1cm x 7.5cm x 0.2cm). To avoid motor or visual confounds, tools and non-tool pairs were
138 carefully matched in terms of visual properties and kinematic requirements as much as possible.
139 Specifically, non-tools were comprised of three cylindrical shapes (adapted from Brandi et al.,
140 2014) with handle, neck and functional-end dimensions matched to each tool they controlled for,
141 ensuring that grip size was matched between tool and non-tool pairs. In addition, all objects had
142 small black stickers placed at pre-specified locations to indicate grasp points, ensuring that grasp
143 position/reach-distance were identical between tool and non-tool pairs regardless of side to be
144 grasped. To avoid familiarity confounds between tools and non-tool control stimuli we chose to
145 use bars instead of scrambled tools and thus, our control non-tools were familiar, but had no
146 specific associated function. Furthermore, each tool and non-tool pair were carefully matched for
147 elongation so that any differences between conditions could not be explained by low-level shape
148 preferences (e.g., Sakuraba et al., 2012; Brandi et al., 2014).

149

150 **Real action setup and apparatus.** Participants were scanned in complete darkness using a
151 head-tilted configuration that allowed direct viewing of the workspace and 3D stimuli without the
152 use of mirrors (Fig. 1B) by tilting the head coil \sim 20° and padding the underside of each
153 participants heads with foam cushions (NoMoCo Pillow, La Jolla, CA, USA). Objects were placed
154 by an experimenter on a turntable above the participant's pelvis and were only visible when

155 illuminated (e.g., Fernández-Espejo et al., 2015; Fig. 1B). All stimuli were mounted such that they
156 were aligned with participants' midlines, never changed position while visible and were tilted
157 away from the horizontal at an angle ($\sim 15^\circ$) to maximize visibility and grasp comfort. For stimulus
158 presentation, the workspace and object were illuminated from the front using a bright white Light
159 Emitting Diode (LED) attached to a flexible plastic stalk (Loc-line, Lockwood Products; Fig. 1B).
160 To control for eye movements, participants were instructed to fixate a small red LED positioned
161 above and behind objects such that they appeared in the lower visual field (Rossit et al., 2013).
162 Throughout the experiment, participants' right eye and arm movements were monitored online
163 and recorded using two MR-compatible infrared-sensitive cameras (MRC Systems GmbH) to
164 verify that participants performed the correct grasping movement (hand camera positioned over
165 the left shoulder; Fig. 1B) and maintained fixation (eye camera beside the right eye; Fig. 1B).
166 The likelihood of motion artefacts related to grasping was reduced by restraining the upper-right
167 arm and providing support with additional cushions so that movements were performed by flexion
168 around the elbow only (Culham, 2006). Auditory instructions were delivered to the participants
169 through earphones (Sensimetrics MRI-Compatible Insert Earphones Model S14, USA). At the
170 beginning of the real action session, participant setup involved adjusting the exact position of: 1)
171 stimuli and the hand to ensure reachability (average grasping distance between the "home"
172 position and object = 43cm), 2) the illuminator to equally light all objects, 3) the fixation LED to
173 meet the natural line of gaze (average distance from fixation to bridge nose = 91cm; visual angle
174 = $\sim 20^\circ$) and 4) the infrared-sensitive eye and hand cameras to monitor eye and hand movement
175 errors. The experiment was controlled by a Matlab script (The MathWorks, USA R2010a) using
176 the Psychophysics Toolbox (Brainard, 1997).

177

178 **Real action experimental paradigm.** We used a powerful block-design fMRI paradigm, that
179 maximised the contrast-to-noise ratio to generate a reliable estimate of the average response
180 pattern (Mur et al., 2009) and improved detection of blood oxygenation level-dependent (BOLD)
181 signal changes without significant interference from artefacts during overt movement (Birn et al.,
182 2004). A block began with an auditory instruction ('Left' or 'Right'; 0.5s) specifying which side of
183 the upcoming object to grasp (Fig. 1C). During the ON-block (10s), the object was briefly

184 illuminated for 0.25s five consecutive times (within 2s intervals) cueing the participant to grasp
185 with a right-handed precision grip (i.e., index finger and thumb) along the vertical axis. Between
186 actions, participants returned their hand to a “home” position with their right hand closed in a fist
187 on their chest (see Fig. 1B). This brief object flashing presentation cycle during ON-blocks has
188 been shown to maximise the signal-to-noise ratio in previous perceptual decoding experiments
189 (Kay et al., 2008; Smith & Muckli, 2010) and eliminates the sensory confound from viewing hand
190 movements (Rossit et al., 2013; Monaco et al., 2015). An OFF-block (10s) followed the
191 stimulation block where the workspace remained dark and the experimenter placed the next
192 stimulus. A single fMRI run included 16 blocks involving the four grasping conditions (i.e., typical
193 tool, atypical tool, right non-tool and left non-tool) each with three repetitions (one per exemplar;
194 every object was presented twice and grasped on each side once). An additional tool (whisk) and
195 a non-tool object were presented on the remaining four blocks per run, but not analysed as they
196 were not matched in dimensions due to a technical problem (the original control non-tool for the
197 whisk was too large to allow rotation of the turntable within the scanner bore). On average
198 participants completed six runs (minimum five, maximum seven) for a total of 18 repetitions per
199 grasping condition. Block orders were pseudorandomised such that conditions were never
200 repeated (two-back) and were preceded an equal number of times by other conditions. Each
201 functional scan lasted 356s, inclusive of start / end baseline fixation periods (14s). Each
202 experimental session lasted ~2.25 hours (including setup, task practice and anatomical scan).
203 Prior to the fMRI experiment, participants were familiarised with the setup and practiced the
204 grasping tasks in a separate lab session (30 minutes) outside of the scanner. The hand and eye
205 movement videos were monitored online and offline to identify error trials. Two runs (of two
206 separate participants) from the entire dataset were excluded from further analysis. In one of
207 these blocks the participant failed to follow the grasping task instructions correctly (i.e.,
208 performing alternated left and right grasps) and for the remaining block another participant did
209 not maintain fixation (i.e., made downward saccades toward objects). In the remaining runs that
210 were analysed, participants made performance errors in <1% of experimental trials. The types of
211 errors included: not reaching (3 trials, 2 participants), reaching in the wrong direction (1 trial, 1
212 participant) and downward eye saccades (5 trials, 3 participants). A one-way repeated measures

213 ANOVA with 12 levels (i.e., the six exemplars across both left vs right grasping conditions)
214 showed that the percentage of errors were equally distributed amongst trial types regardless of
215 whether the percentage of hand and eye errors were combined or treated separately (all p 's >
216 0.28).

217 Crucially, since the tools' handles were always oriented rightward, the right and left tool
218 trials involved grasping tools either by their handle (typical) or functional-end (atypical),
219 respectively. On the other hand, grasping non-tools did not involve a typical manipulation but
220 only differed in grasp direction with right vs left grasps (Fig. 1C). We chose to present rightward
221 oriented tool handles only, rather than alternate object orientation randomly between trials, to
222 reduce total trial numbers (scanning times was already quite extensive with set-up) and due to
223 technical limitations (i.e., the turntable's rotation direction was fixed and it was difficult for the
224 experimenter to manipulate tool orientation in the dark). Nevertheless, by comparing the
225 decoding accuracies for each region between tool and non-tool grasps (which were matched for
226 biomechanics) we ruled out the possibility that our typically manipulation simply reflected grasp
227 direction. Specifically, we took the conservative approach that for an area to be sensitive to tool
228 grasping typicality, it should not only show greater-than-chance decoding for typical vs atypical
229 actions with tools (i.e., typicality), but also that the typicality decoding accuracy should be
230 significantly greater than accuracy for biomechanically matched actions with our control non-tools
231 (i.e. right vs left actions with non-tools).

232

233 **Visual Localizer.** On a separate day from the real action experiment, participants completed a
234 Bodies, Chairs, Tools and Hands (BOTH) visual localizer (adapted from Bracci et al., 2012; 2013;
235 2016) using a standard coil configuration (see MRI acquisition for details). Two sets of exemplar
236 images were selected from previous stimuli databases (Bracci et al., 2012; 2013; 2016) that were
237 chosen to match, as much as possible, the characteristics within the tool (i.e., identity &
238 orientation), body (i.e., gender, body position & amount of skin shown), hand (i.e., position &
239 orientation) and chair (i.e., materials, type & style) categories. Using a mirror attached to the
240 head coil, participants viewed separate blocks (14s) of 14 different grayscale 2D pictures from a
241 given category (400 x 400 pixels; 0.5s). Blank intervals separated individual stimuli (0.5s) and

242 scrambled image blocks separated cycles of the four randomised category blocks (Fig. 1D).
243 Throughout, participants fixated a superimposed bullseye on the centre of each image and, to
244 encourage attention, performed a one-back repetition detection task where they made a right-
245 handed button press whenever 2 successive photographs were identical. The 2D images stimuli
246 were presented with an LCD projector (SilentVision SV-6011 LCD, Avotech Inc.). A single fMRI
247 run included 24 category blocks (6 reps per condition) with blank fixation baseline periods (14s)
248 at the beginning and the end of the experiment. Each localizer scan lasted 448s and, on
249 average, participants completed 4 runs (minimum 3, maximum 4) for a total of 24 reps per
250 condition. The entire localizer session lasted ~50 minutes after including the time taken to
251 acquire a high-resolution anatomical scan and setup participants.

252

253 **MRI Acquisition.** The BOLD fMRI measurements were acquired using a 3T wide bore GE-750
254 Discovery MR scanner at the Norfolk & Norwich University Hospital (Norwich, UK). To achieve a
255 good signal to noise ratio during the real action fMRI experiment, the posterior half of a 21-
256 channel receive-only coil was tilted and a 16-channel receive-only flex coil was suspended over
257 the anterior-superior part of the skull (see Fig. 1B). A T2*-weighted single-shot gradient Echo-
258 Planer Imaging (EPI) sequence was used throughout the real action experiment to acquire 178
259 functional MRI volumes (Time to Repetition (TR) = 2000ms; Voxel Resolution (VR) = 3.3 x 3.3 x
260 3.3mm; Time to Echo (TE) = 30ms; Flip Angle (FA) = 78°; Field of View (FOV) = 211x 211mm;
261 Matrix Size (MS) = 64 x 64) that comprised 35 oblique slices (no gap) acquired at 30° with
262 respect to AC-PC, to provide near whole brain coverage. A T1-weighted anatomical image with
263 196 slices was acquired at the beginning of the session using BRAVO sequences (TR = 2000ms;
264 TE = 30ms; FOV = 230mm x 230mm x 230mm; FA = 9°; MS = 256 x 256; Voxel size = 0.9 x 0.9
265 x 0.9mm).

266 For visual localizer sessions, a full 21-channel head coil was used to obtain 224
267 functional MRI volumes (Time to Repetition (TR) = 2000ms; Voxel Resolution (VR) = 3.3 x 3.3 x
268 3.3mm; Time to Echo (TE) = 30ms; Flip Angle (FA) = 78°; Field of View (FOV) = 211x 211mm;
269 Matrix Size (MS) = 64 x 64). A high resolution T1-weighted anatomical image with 196 slices was
270 acquired before the localizer runs (TR = 2000ms; TE = 30ms; FOV = 230mm x 230mm x

271 230mm; FA = 9°; MS = 256 x 256; Voxel size = 0.9 x 0.9 x 0.9mm). Localizer datasets for two
272 participants were retrieved from another study from our group (Rossit et al., 2018) where the
273 identical paradigm was performed when acquiring volumes using a Siemens whole-body 3T
274 MAGNETOM Prisma fit scanner with a 64-channel head coil and integrated parallel imaging
275 techniques at the Scannexus imaging centre (Maastricht, The Netherlands) and comparable
276 acquisition parameters (Functional scans: TR = 2000ms; TE = 30ms; FA = 77°; FOV = 216mm;
277 MS = 72 x 72; Anatomical scan: T1-weighted anatomical image: TR = 2250ms; TE = 2.21ms; FA
278 = 9°; FOV = 256 mm; MS = 256 x 256).

279

280 **Data Preprocessing.** Preprocessing and ROI definitions were performed using BrainVoyager
281 QX (version 2.8.2) (Brain Innovation, Maastricht, The Netherlands). BrainVoyager's 3D motion
282 correction (sinc interpolation) aligned each functional volume within a run to the functional
283 volume acquired closest in time to the anatomical scan (e.g., Rossit et al., 2013). Slice scan time
284 correction (ascending and interleaved) and high-pass temporal filtering (2 cycles/run) was also
285 performed. Functional data were superimposed on to the anatomical brain images acquired
286 during the localizer paradigm that were previously aligned to the plane of the anterior-posterior
287 commissure and transformed into standard stereotaxic space (Talairach, & Tournoux, 1988).
288 Excessive motion was screened by examining the time-course movies and motion plots created
289 with the motion-correction algorithms for each run. No spatial smoothing was applied.

290 To estimate activity in the localizer experiment, a predictor was used per image condition
291 (i.e., Bodies, Objects, Tools, Hands and Scrambled) in a single-subject general linear model
292 (GLM). Predictors were created from boxcar functions that were convolved with a standard 2y
293 model of the hemodynamic response function (Boynton et al., 1996) and aligned to the onset of
294 the stimulus with durations matching block length. The baseline epochs were excluded from the
295 model, and therefore, all regression coefficients were defined relative to this baseline activity.
296 This process was repeated for the real action experiment, using 16 separate predictors for each
297 block of stimulation independently per run (12 exemplars - knife typical, knife atypical, spoon
298 typical etc. plus 4 foil trials) and 6 motion regressors (confound predictors). These estimates
299 (beta weights) from the real action experiment were used as the input to the pattern classifier.

300 **Visual Localizer Regions of interest (ROIs).** Twelve visual ROIs were defined at the individual
301 participant level from the independent BOTH localizer data by drawing a cube (15 voxels³)
302 around the peak of activity from previously reported volumetric contrasts (see list below; Fig. 1E;
303 Table 1) set at a threshold of $p < .005$ (Gallivan et al., 2013) or, if no activity was identified, of $p <$
304 $.01$ (Bracci et al., 2016). In cases where no activity was observed, the ROI was omitted for that
305 participant (see Table 1). Given the predominantly left lateralised nature of tool-processing
306 (Lewis, 2006), all individual participant ROIs were defined in the left hemisphere (Bracci et al.,
307 2012; 2013; 2016; Peelen et al., 2013). Six tool-selective ROIs commonly described in left
308 frontoparietal and occipitotemporal cortices were identified by contrasting activation for tool
309 pictures vs other object pictures (IPS-Tool; SMG; dorsal and ventral Premotor Cortex (PMd;
310 PMv), LOTC-Tool; pMTG; Martin et al., 1996; Grafton et al., 1997). Moreover, two hand-selective
311 ROIs were identified in LOTC (LOTCH-Hand) and IPS (IPS-Hand) by contrasting activation for
312 hand pictures vs pictures of other body parts (Bracci et al., 2012; 2016; 2018; Peelen et al.,
313 2013; Palser & Cavina-Pratesi, 2018). Additionally, we defined a body-selective (LOTCH-Body;
314 Bodies > Chairs; Bracci & de Beeck, 2016), two object-selective ROIs (LOTCH-Object; posterior
315 Fusiform, pFs; Chairs > Scrambled; Bracci & de Beeck, 2016; Hutchison et al., 2014) and an
316 Early Visual Cortex ROI (EVC; All Categories > Baseline; Bracci & de Beeck, 2016). The ROI
317 locations were verified by a senior author (S.R.) with respect to the following anatomical
318 guidelines and contrasts:

- 319 • Lateral Occipitotemporal Cortex-Object selective (LOTCH-Object) - (Chairs > Scrambled)
320 (Hutchison et al., 2014; Bracci & de Beeck, 2016) - defined by selecting the peak of
321 activation near the Lateral Occipital Sulcus (LOS; Hutchison et al., 2014; Bracci & de
322 Beeck, 2016; Malach et al., 1995; Grill-Spector et al., 1999; 2001).
- 323 • Lateral Occipitotemporal Cortex-Body selective (LOTCH-Body) - (Bodies > Chairs) (Bracci
324 & de Beeck, 2016) - defined by selecting the peak of activation near the LOS and inferior
325 to the left Extrastriate Body Area (EBA; Valyear & Culham, 2010) which was identified by
326 the contrast ((Bodies + Hands) > Chairs) (adapted from Bracci, et al., 2010; ((Whole
327 Bodies + Body Parts) > (Hands + Chairs))). EBA was not included in the analysis.

- 328 • Lateral Occipitotemporal Cortex-Hand selective (LOTC-Hand) - ((Hands > Chairs) AND
329 (Hands > Bodies)) (Bracci & de Beeck, 2016) - defined by selecting the peak of activation
330 near the LOS. These were often anterior to LOTC-Body (Bracci et al., 2010; 2016).
- 331 • Lateral Occipitotemporal Cortex-Tool selective (LOTC-Tool) - (Tools > Chairs) (Bracci, et
332 al., 2012; Hutchison et al., 2014) - defined by selecting the peak of activation near the
333 LOS. These often closely overlapped LOTC-Hand (Bracci, et al., 2012).
- 334 • Posterior Middle Temporal Gyrus (pMTG) - (Tools > Chairs) (Hutchison, et al., 2014;
335 Valyear & Culham, 2010) – defined by selecting the peak of activation on the pMTG,
336 more lateral, ventral and anterior to EBA (Hutchison et al., 2014). We selected the peak
337 anterior to the Anterior Occipital Sulcus (AOS), as the MTG is in the temporal lobe and
338 the AOS separates the temporal from the occipital (Damasio, 1995).
- 339 • Posterior Fusiform Sulcus (pFs) - (Chairs > Scrambled) (Hutchison, et al., 2014) - defined
340 by selecting the peak of activation in the posterior aspect of the fusiform gyrus, extending
341 into the occipitotemporal sulcus (Hutchison, et al., 2014).
- 342 • Intraparietal Sulcus-Hand selective (IPS-Hand) - (Hands > Chairs) (Bracci, et al. 2016;
343 Bracci & de Beeck, 2016) – defined by selecting the peak of activation on the IPS (Bracci
344 & de Beeck, 2016).
- 345 • Intraparietal Sulcus-Tool selective (IPS-Tool) - (Tools > Scrambled) (Bracci, et al., 2016;
346 Bracci et al., 2016) - defined by selecting the peak of activation on the IPS (Bracci & Op
347 de Beeck, 2016).
- 348 • Supramarginal Gyrus (SMG) - (Tools > Scrambled) (Creem-Regehr, et al., 2007) -
349 defined by selecting the peak of activation located most anterior along the SMG (Peeters,
350 et al., 2013), lateral to the anterior segment of the IPS (Gallivan, et al., 2013), posterior to
351 the Precentral Sulcus (PreCS) and superior to the lateral sulcus (Ariani, et al., 2015).
- 352 • Dorsal Premotor Cortex (PMd) - (Tools > Scrambled) - defined by selecting the peak of
353 activation at the junction of the PreCS and the superior frontal sulcus (Gallivan et al.,
354 2013; Ariani, et al., 2015).

- 355 • Ventral Premotor Cortex (PMv) - (Tools > Scrambled) (Creem-Regehr, et al., 2007) -
356 defined by selecting the voxels inferior and posterior to the junction between the inferior
357 frontal sulcus and the PreCS (Gallivan et al., 2013).
- 358 • Early Visual Cortex (EVC) - (All Conditions > Baseline) (Bracci & de Beeck, 2016) -
359 defined by selecting the voxels in the occipital cortex near the calcarine sulcus (Singhal,
360 et al., 2013).

361

362 *****

363 Please insert Table 1 here

364 *****

365

366 **Pattern Classification.** We performed MVPA independently for tool and non-tool trial types.
367 Independent linear pattern classifiers (linear Support Vector Machine; SVM), were trained to
368 learn the mapping between a set of brain-activity patterns (beta values computed from single
369 blocks of activity) from the visual ROIs and the type of grasp being performed with the tools
370 (typical vs atypical) or non-tools (right vs left). To test the performance of our classifiers,
371 decoding accuracy was assessed using an n-fold leave-one-run-out cross validation procedure;
372 thus, our models were built from n – 1 runs and were tested on the independent nth run
373 (repeated for the n different possible partitions of runs in this scheme (Duda et al., 2001; Smith et
374 al., 2010; 2015; Gallivan et al., 2016) before averaging across n iterations to produce a
375 representative decoding accuracy measure per participant and per ROI. Beta estimates for each
376 voxel were normalised (separately for training and test data) within a range of -1 to +1 before
377 input to the SVM (Chang & Lin, 2011) and the linear SVM algorithm was implemented using the
378 default parameters provided in the LibSVM toolbox (C = 1). Pattern classification was performed
379 with a combination of in-house scripts (Smith et al., 2010; 2015) using Matlab with the Neuroelf
380 toolbox (version 0.9c; <http://neuroelf.net>) and a linear SVM classifier (libSVM 2.12 toolbox;
381 <https://csie.ntu.edu.tw/~cjlin/libsvm>).

382

383 **Statistical Analysis.** One-tailed one-sample t-tests were used to test for above chance decoding
384 for tool and non-tool action classifications in every ROI independently. If the pattern of results
385 was consistent with our hypothesis (i.e., decoding accuracy was significantly above chance for
386 tools, but not non-tools), we further ran a one-tailed pairwise t-tests to compare if decoding
387 accuracy was significantly higher for tools than non-tools. Additionally, to test for differences in
388 decoding accuracy between ROIs we used repeated measures 2 x 2 ANOVAs with ROI (tool vs
389 hand selective) and object category (tool vs non-tool) as within-subject factors. Then, to test if
390 univariate differences would differ between grasp types for the tools, but not non-tools we ran 2 x
391 2 ANOVAs with grasp type (typical/right vs atypical/left) and object category (tools vs non-tools)
392 by entering mean beta weights for each ROI. Separately for each set of analyses we corrected
393 for multiple comparisons with False Discovery Rate (FDR) correction of $q \leq 0.05$ (Benjamini &
394 Hochberg, 1995; Benjamini & Yekutieli, 2001) across the number of tests. Only significant results
395 are reported (see Fig. 2). Our sample size was based on similar motor studies using MVPA (e.g.,
396 Ariani et al., 2015; 2018; Gallivan et al., 2009; 2013; 2014), though no power analysis was
397 performed prior to data collection.

398 To test for evidence for the null hypothesis over an alternative hypothesis, we
399 supplemented null-hypothesis significance tests with Bayes factors (BF; Wagenmakers, 2007;
400 Rouder et al., 2009). Bayes factors were estimated using the bayesFactor toolbox in Matlab
401 (version 1.1; <https://klabhub.github.io/bayesFactor>). The Jeffreys–Zellner–Siow default prior on
402 effect sizes was used (Rouder, Morey, Speckman, & Province, 2012) and BF's were interpreted
403 according to criteria set out by Jeffreys (1961; cited from Jarosz & Wiley, 2014) where a BF_{01}
404 between 1-3 and > 3 indicates 'anecdotal' and 'substantial' evidence in favour of the null,
405 respectively.

406

407 **Data Availability.** Stimuli, code for running experiment and for MVPA analyses and ROI data are
408 accessible from Open Science Framework at: <https://osf.io/zxnpv>. Full raw MRI dataset (real
409 action and visual localizer) is accessible from OpenNEURO at:
410 <https://openneuro.org/datasets/ds003342/versions/1.0.0>.

411

412 **Results**

413 In line with our predictions, as can be seen in Fig. 2, a one-sample t-test against chance (50%)
 414 showed that SVM decoding accuracy (FDR-corrected) from hand-selective ROIs in LOTC and
 415 IPS were significantly greater-than-chance when discriminating typical vs atypical actions with
 416 tools (LOTC-Hand accuracy = 56% \pm (SD) 0.9%, $t(16) = 2.73$, $p = 0.007$, $d = 0.66$; IPS-Hand
 417 accuracy = 57% \pm 0.11%, $t(18) = 2.72$, $p = 0.007$, $d = 0.62$), but not biomechanically-matched
 418 actions with non-tools (right vs left; LOTC-Hand: $p = 0.252$, IPS-Hand: $p = 0.844$). In fact, there
 419 was substantial evidence in favour of null decoding of non-tool actions for the IPS ROI (LOTC-
 420 Hand: $BF_{01} = 2.29$; IPS-Hand = 8.4). Importantly, results from a stringent between-classification
 421 paired samples t-test also further supported this: typicality decoding accuracy from both LOTC-
 422 Hand and IPS-Hand was significantly higher for tools than for biomechanically-matched actions
 423 with non-tools (LOTC-Hand: $t(16) = 2.11$, $p = 0.026$, $d = 0.51$; IPS-Hand: $t(18) = 3.26$, $p = 0.002$,
 424 $d = 0.75$; Fig. 2A and Fig. 2B).

425

426

427

Please insert Figure 2 here

428

429

430 No other visual ROI, including tool-selective areas, displayed the same significant effects
 431 as hand-selective areas (Fig. 2A and Fig. 2B). For tool-selective ROIs, decoding accuracy was
 432 not significantly greater-than-chance for classifying actions with tools or non-tools (all p 's >
 433 0.024), with the Bayesian approach demonstrating strong evidence in favour of the null for PMv
 434 (tool: $BF_{01} = 3.23$; non-tool: $BF_{01} = 6.85$) and SMG tool decoding (tool: $BF_{01} = 8.85$; other BF_{01} 's <
 435 1.08). The exception to this was tool-selective PMd which was found to decode significantly
 436 above chance actions with non-tools (accuracy = 59% \pm 0.08% $t(13) = 4.11$, $p = 0.001$, $d = 1.1$;
 437 Fig. 2A), but not tools ($BF_{01} = 4.42$). As for object- and body-selective areas, LOTC-Object
 438 decoding accuracy did not differ from chance for tools or non-tools ($p > 0.026$), though evidence
 439 in favour of the null was anecdotal (BF_{01} 's < 1.33), whereas pFs and LOTC-Body decoded
 440 actions above chance with both tools (pFs: accuracy = 58% \pm 0.14% $t(18) = 2.57$, $p = 0.01$, $d =$

441 0.59; LOTC-Body: accuracy = 59% \pm 0.08% ($t(17) = 4.75$, $p < 0.001$, $d = 1.12$) and non-tools
442 (pFs: accuracy = 57% \pm 0.12% $t(18) = 2.59$, $p = 0.009$, $d = 0.59$; LOTC-Body: accuracy = 56% \pm
443 0.10% ($t(17) = 2.46$, $p = 0.012$, $d = 0.58$; Fig. 2A). Like many of the tool-selective ROIs, the
444 control EVC ROI was not found to decode actions with either type of object (p 's < 0.026), albeit
445 evidence in favour of the null was anecdotal (BF_{01} 's > 0.37).

446 Since we obtained a different pattern of results for LOTC and IPS ROIs that were hand-
447 vs tool-selective, we compared the decoding accuracies between these regions with a repeated
448 measures ANOVA with ROI (hands vs tool-selective) and object category (tool vs non-tools) as
449 within-factors. As shown in Fig. 2B, there was a significant interaction between ROI and object
450 category in IPS ($F(1, 18) = 5.94$, $p = 0.025$, $\eta^2 = 0.25$). Post-hoc t-tests showed that for IPS-Hand,
451 grasp type decoding was significantly higher for tools than non-tools (mean difference = 0.1%,
452 SE = 0.03%; $p = 0.004$), but not for IPS-Tool (mean difference = 0.02%, SE = 0.03%). However,
453 for LOTC this interaction was not significant ($p = 0.379$; Fig. 2B), nor were the remaining main
454 effects (all p 's > 0.367).

455 Next, we examined whether significant decoding in hand-selective cortex could be
456 accounted for by low-level sensory differences between the tools' handles and functional-ends.
457 First, to test the possibility that tool-specific decoding in hand-selective cortex could be driven by
458 simple textural differences (e.g., a smooth handle vs a serrated knife blade), we repeated the
459 analysis using a left somatosensory cortex ROI (SC; defined by selecting the peak voxel in the
460 postcentral gyrus in the same subjects with an independent univariate contrast of All Grasps $>$
461 Baseline; Fabbri et al., 2014, 2016). However, unlike the higher accuracies for grasping tools
462 than non-tools in the hand-selective ROIs, grasp type decoding in SC was significantly greater-
463 than-chance for both tool (accuracy = 57% \pm 0.11%, $t(18) = 3.04$, $p = 0.004$, $d = 0.7$) and non-
464 tools (accuracy = 57% \pm 0.09% $t(18) = 3.45$, $p = 0.001$, $d = 0.79$; Fig. 2C). This indicates that
465 tool-specific decoding in hand-selective cortex cannot be solely explained by somatosensory
466 differences in the stimuli. Second, we tested if size differences between our objects, and thus
467 grip size, could drive tool-specific decoding in hand-selective cortex (i.e., the functional-end of
468 the tool being wider than its handle for the spoon and pizza cutter). As shown in Fig. 3A, we
469 decoded smaller vs larger objects in three separate decoding analysis, regardless of whether the

470 objects were tools or non-tools. Each separate grip size pair decoding analysis is shown in each
 471 row of images of Fig. 3A (from top to bottom: small vs medium; small vs large; medium vs large).
 472 Decoding accuracies for each grip size pair were then averaged and tested against chance
 473 using a one-tailed one-sample t-test. Decoding of grip size was not significant for any visual ROI
 474 (all p 's ≥ 0.1 ; Fig. 3B) and evidence in favour of the null was strong for most ROIs including IPS-
 475 Hand ($BF_{01} = 8$), EVC ($BF_{01} = 3.22$), LOTC-Object ($BF_{01} = 4.93$), pFs ($BF_{01} = 5.97$), SMG ($BF_{01} =$
 476 3.33), PMv ($BF_{01} = 3.91$) and PMd ($BF_{01} = 3.56$; all other BF_{01} 's > 1.84). Taken together, these
 477 findings suggest that hand-selective regions, particularly in the IPS, are sensitive to whether a
 478 tool is grasped correctly by its handle or not, and that these effects are not simply due to textural
 479 or size differences between the stimuli used or actions performed.

480 In addition, we found that the significant decoding accuracies reported here do not simply
 481 reflect the overall response amplitudes within each ROI. When we analysed the mean beta
 482 weights in ANOVAs with grasp type and object category as within-subject factors for each ROI
 483 (i.e., as done in conventional univariate analysis; see Fig. 4), the only significant effect observed
 484 was a main effect of object category (unrelated to typicality), where greater activation was found
 485 for tools relative to non-tools in LOTC-Tool ($F(1,16) = 9.25$, $p = 0.008$, $\eta^2 = 0.37$; mean difference
 486 $= 0.1$, $SE = 0.03$), pFs ($F(1,18) = 8.68$, $p = 0.009$, $\eta^2 = 0.33$; mean difference $= 0.07$, $SE = 0.02$)
 487 and SMG ($F(1,16) = 10.5$, $p = 0.005$, $\eta^2 = 0.4$; mean difference $= 0.089$, $SE = 0.03$).

488

489

490

Please insert Figures 3 and 4 here

491

492

493 Discussion

494 Our understanding of how the human brain represents object properties (Kanwisher, 2010) and
 495 simple hand movements (Gallivan & Culham, 2015) has significantly advanced in the last few
 496 decades, however, far less is known about the neural representations that underpin real actions
 497 involving 3D tools (Valyear et al., 2017). Most neuroimaging experiments that investigate how
 498 tools and their associated actions are represented in the brain have used visual paradigms

499 where objects and body-parts are displayed as 2D images (Ishibashi et al., 2016). These studies
500 have discovered a tight anatomical and functional relationship between hand- and tool-selective
501 areas in LOTC and IPS, thought to reflect action-related processing, however this was yet to be
502 directly tested (Bracci et al., 2012; 2013; 2016; Peelen et al., 2013; Striem-Amit et al., 2017;
503 Maimon Mor, 2020). Here we defined visually category-selective areas and investigated if they
504 were sensitive to real action affordances involving 3D tools. We found the first evidence that
505 hand-selective cortex (left IPS-Hand and LOTC-Hand) represents whether a 3D tool is being
506 grasped appropriately by its handle. Remarkably, the same effects were not observed in tool-,
507 object-, or body-selective areas, even when these areas overlapped with hand-selective voxels in
508 IPS and LOTC.

509 Our results indicate that visual hand-selective areas in parietal and occipital cortices
510 process sensorimotor affordances of typicality for hand movements with 3D tools. Importantly,
511 these action-related representations were detected exclusively for actions with tools, but not for
512 biomechanically matched actions with non-tools. This tool-specificity was particularly evident in
513 IPS-hand because Bayesian evidence demonstrated that decoding of grasp type with non-tools
514 was not possible. In a similar vein, while the IPS ANOVA demonstrated boosted tool-specific
515 decoding specifically for the hand-selective ROI, this effect was not significant in LOTC. This
516 suggests that typicality effects may be less robust for LOTC-hand. Our findings shed light into the
517 features of sensorimotor processing in hand-selective areas. First, their representations are
518 sensitive to concepts acquired through experience (i.e., knowing how to grasp tools appropriately
519 is a learnt skill; Martin, 2007), fitting with evidence showing that learning about how to manipulate
520 tools (Weisberg et al., 2007) or even performing such actions (Valyear et al., 2012; Brandi et al.,
521 2014; Styrkowiec et al., 2019) affects LOTC and IPS activity. For example, our results are
522 compatible with those from Brandi et al. (2014) who showed coactivation of these regions during
523 'use' actions of tools/non-tools. Our results, however, additionally suggest that this learnt
524 information, at least for grasping, is coded in specific category-selective parts of LOTC and IPS.
525 Second, information processed by hand-selective cortex is represented in an abstract format
526 beyond low level properties (e.g., basic kinematics), since Bayesian evidence strongly suggested
527 that decoding grip size was not possible. This fits well with reports that hand-/tool-selective

528 overlap exists in people born without vision (Peelen et al., 2013) or without hands (Striem-Amit et
529 al., 2017) suggesting that their development is driven by similarities in how they process non-
530 sensory tool information. In addition, our data also resonates with previous studies showing that
531 tool-selective areas in pMTG/LOTC and IPS represent abstract action goals (reach vs grasp)
532 regardless of biomechanics (Gallivan et al., 2013; Jacobs et al., 2010), albeit our findings were
533 observed for hand-selective areas only. Third, our study shows that these high-level
534 representations are automatically evoked (Valyear et al., 2012) as throughout the real-action
535 fMRI task there was no explicit requirement to use the tools and participants were never told that
536 we were investigating 'tools'. Here we demonstrate that these principles, frequently described to
537 support tool-use (Gibson, 1979; Imamizu et al., 2003; Maravita & Iriki 2004; Umiltà et al., 2008;
538 Lingnau & Downing, 2015), apply to brain areas specialised for representing the human hand,
539 our primary *tool* for interacting with the world.

540 An intriguing aspect of our results is that typicality decoding was successful using activity
541 patterns from hand-selective, but not overlapping parts of tool-selective cortex in the LOTC and
542 IPS. Bayesian evidence only anecdotally supported the possibility that decoding was null from
543 tool-selective areas, but significantly stronger typicality decoding was observed for IPS-Hand
544 than IPS-Tool during tool, but not non-tool grasps. In contrast to previous picture viewing fMRI
545 studies showing that overlapping hand- and tool-selective regions exhibit similar responses
546 (Bracci et al., 2012; 2013; 2016), our findings uniquely support previous speculations that hand-
547 selective IPS, and possibly LOTC, could be functionally distinct from tool-selective regions
548 despite their anatomical overlap (e.g., Striem-Amit et al., 2017). This pattern of results is unlikely
549 to be driven by differences in ROI radius (Etzet et al., 2013) since voxel size differences were
550 negligible between hand- and tool-selective ROIs (mean difference: IPS: 29; LOTC: 4). In fact, if
551 category-related results were merely caused by ROI size, then significant decoding should have
552 also been observed in the much larger LOTC-Object ROI (see Table 1). Alternatively, successful
553 higher decoding in hand than tool-selective areas might reflect that our task simply required
554 grasping-to-touch the tools, rather than their utilisation. That is, coding in category-selective
555 areas might operate in an effector-dependent manner, akin to how tool-selective pMTG/LOTC
556 codes the type of action being performed when holding a pair of tongs, but not if being performed

557 by the hand alone (Gallivan et al., 2013). In line with this interpretation, neural representations in
558 LOTC-Hand of one-handed amputees are also known to become richer as prosthetic usage
559 increases (Van den Heiligenberg 2018), which, again, indicates that the representations in hand-
560 selective cortex depend on effector use. An alternative, but not mutually exclusive, possibility is
561 that only tool-use actions elicit tool-selective representations (see Randerath et al., 2010)
562 because of the cognitively taxing demands these complex actions rely on, such as retrieving
563 knowledge about manipulation hierarchies (Buxbaum, 2017) or the laws that constrain object
564 movement (Fischer et al., 2016). In either case, the specificity of decoding typical tool grasps in
565 hand-, rather than tool- and hand-, selective cortex challenges the popular interpretation that
566 brain activation for viewing tool images is a reflection of sensorimotor processing linked to tool
567 manipulation (Martin et al., 1996; Mahon et al., 2007; Fang & He, 2005; Grafton et al., 1997;
568 Martin & Chao, 2001; also see Mahon & Caramazza, 2009).

569 There are several differences between our study and previous research. First our
570 univariate analysis revealed no relationship between mean activity and typicality. Previous
571 studies have found greater univariate activation in occipito-temporal and/or fronto-parietal cortex
572 for typical relative to atypical actions when participants viewed pictures and movies or
573 pantomimed (Johnson-Frey et al., 2003; Valyear & Culham, 2010; Yoon et al., 2012; Mizelle et
574 al., 2013; Przybylski & Króliczak, 2017). Our results fit the claim that MVPA can reveal fine-
575 grained effects (Kriegeskorte, et al., 2006), as recently argued by Buchwald et al. (2018) when
576 showing that pantomimed typical tool vs non-tool grasps could be decoded from a range of
577 regions including premotor and intraparietal areas. We suspect that task differences are also an
578 important contributing factor to the general lack of univariate effects. For example, our
579 experiment involved fewer, less varied, exemplars than in these previous picture studies.
580 Likewise, our grasp-to-touch paradigm is simpler than studies showing greater univariate
581 activations in the left SMG, premotor cortex, LOTC and IPS when performing real tool-use
582 actions (Brandi et al., 2014; Valyear et al., 2012) or haptically-guided typical tool grasps
583 (Styrkowiec et al., 2019) relative to tool/non-tool control actions. Finally, in our study, grasping
584 always involved a precision grip whereas previous studies employed power grasps which are
585 better suited for certain actions with some specific tools. This factor may have led to the lack of

586 typically decoding effects in tool-selective cortex as these areas could be sensitive to both the
587 side of the object being grasped and the function of particular grips (Buxbaum et al., 2006). We
588 designed our precision grasping task to investigate tool affordances while carefully equating
589 biomechanics between actions, such that decoding typicality was unlikely to be attributed to
590 motor-related differences. Future real action studies manipulating the type of grasp (e.g., grasp
591 vs use) are needed to further identify the content of information coded by visual hand-/tool-
592 selective areas.

593 It is worth noting that we were unable to match the visual symmetry between object
594 categories (our tools were asymmetric while the non-tools were symmetric) because asymmetric
595 non-tool bars were perceived as tools by participants (i.e., the wider side perceived as a
596 functional-end). Nonetheless, tool-specific decoding in hand-selective cortex is unlikely to be
597 explained by simple effects of symmetry: if effects were related to symmetry comparable
598 decoding effects should have been observed in symmetry-responsive regions (e.g., LOTC-
599 Object; EVC; Beck, et al., 2006), particularly since they are also known to code motor-related
600 information (e.g., Gallivan & Culham, 2015; Monaco et al., 2020).

601 In conclusion, parietal and occipital visual regions specialised for representing hands
602 were found to encode information about the functional relationship between the grasping hand
603 and a tool, implicating hand-selective cortex in motor control. These findings raise novel
604 questions about the possibility that overlapping hand- and tool-selective regions are functionally
605 distinct and begin to uncover which brain regions evolved to support tool-use, a defining feature
606 of our species.

607

608 **REFERENCES**

- 609 Ambrose, S. H. (2001). Paleolithic technology and human evolution. *Science*, 291(5509), 1748-
610 1753.
- 611 Ariani, G., Oosterhof, N. N., & Lingnau, A. (2018). Time-resolved decoding of planned delayed
612 and immediate prehension movements. *Cortex*, 99, 330-345.
- 613 Ariani, G., Wurm, M. F., & Lingnau, A. (2015). Decoding internally and externally driven
614 movement plans. *J Neurosci*, 35(42), 14160-14171.

- 615 Astafiev, S. V., Stanley, C. M., Shulman, G. L., & Corbetta, M. (2004). Extrastriate body area in
616 human occipital cortex responds to the performance of motor actions. *Nat Neurosci*, 7(5),
617 542-548.
- 618 Bach, P., Peelen, M. V., & Tipper, S. P. (2010). On the role of object information in action
619 observation: an fMRI study. *Cereb Cortex*, 20(12), 2798-2809.
- 620 Beck, D. M., Pinsk, M. A., & Kastner, S. (2005). Symmetry perception in humans and macaques.
621 *Trends Cogn Sci*, 9(9), 405-406.
- 622 Benjamini, Y., & Hochberg, Y. (1995). Controlling the false discovery rate: a practical and
623 powerful approach to multiple testing. *Journal of the Royal statistical society: Series B*
624 (Methodological), 57(1), 289-300.
- 625 Benjamini, Y., & Yekutieli, D. (2001). The control of the false discovery rate in multiple testing
626 under dependency. *Ann Stat*, 1165-1188.
- 627 Birn, R. M., Cox, R. W., & Bandettini, P. A. (2004). Experimental designs and processing
628 strategies for fMRI studies involving overt verbal responses. *Neuroimage*, 23(3), 1046-
629 1058.
- 630 Boynton, G. M., Engel, S. A., Glover, G. H., & Heeger, D. J. (1996). Linear systems analysis of
631 functional magnetic resonance imaging in human V1. *J Neurosci*, 16(13), 4207-4221.
- 632 Bracci, S., & de Baeck, H. O. (2016). Dissociations and associations between shape and
633 category representations in the two visual pathways. *J Neurosci*, 36(2), 432-444.
- 634 Bracci, S., & Peelen, M. V. (2013). Body and object effectors: the organization of object
635 representations in high-level visual cortex reflects body-object interactions. *J Neurosci*,
636 33(46), 18247-18258.
- 637 Bracci, S., Caramazza, A., & Peelen, M. V. (2018). View-invariant representation of hand
638 postures in the human lateral occipitotemporal cortex. *NeuroImage*, 181, 446-452.
- 639 Bracci, S., Cavina-Pratesi, C., Ietswaart, M., Caramazza, A., & Peelen, M. V. (2012). Closely
640 overlapping responses to tools and hands in left lateral occipitotemporal cortex. *J*
641 *Neurophysiol*, 107(5), 1443-1456.

- 642 Bracci, S., Ietswaart, M., Peelen, M. V., & Cavina-Pratesi, C. (2010). Dissociable neural
643 responses to hands and non-hand body parts in human left extrastriate visual cortex. *J*
644 *Neurophysiol*, 103(6), 3389-3397.
- 645 Brainard, D.H. (1997). The Psychophysics Toolbox. *Spa Vis*, 10(4), 433-436.
- 646 Brandi, M. L., Wohlschläger, A., Sorg, C., & Hermsdörfer, J. (2014). The neural correlates of
647 planning and executing actual tool use. *J Neurosci*, 34(39), 13183-13194.
- 648 Buxbaum, L. J. (2017). Learning, remembering, and predicting how to use tools: Distributed
649 neurocognitive mechanisms: Comment on Osiurak and Badets (2016). *Psychol Rev*,
650 124(3), 346-360.
- 651 Buxbaum, L. J., Kyle, K. M., Tang, K., & Detre, J. A. (2006). Neural substrates of knowledge of
652 hand postures for object grasping and functional object use: Evidence from fMRI. *Brain*
653 *research*, 1117(1), 175-185.
- 654 Chang, C. C., & Lin, C. J. (2011). LIBSVM: A library for support vector machines. *ACM*
655 *transactions on intelligent systems and technology (TIST)*, 2(3), 1-27.
- 656 Creem-Regehr, S. H., Dilda, V., Vicchilli, A. E., Federer, F., & Lee, J. N. (2007). The influence of
657 complex action knowledge on representations of novel graspable objects: evidence from
658 functional magnetic resonance imaging. *J Int Neuropsych Soc*, 13(6), 1009-1020.
- 659 Culham, J. C. (2006). Functional neuroimaging: Experimental design and analysis R. Cabeza, A.
660 Kingstone (Eds.), *Handbook of Functional Neuroimaging of Cognition* (2nd ed.), MIT,
661 Cambridge, MA, 53-82.
- 662 Damasio, H. (1995). *Human brain anatomy in computerized images*. New York: Oxford
663 University Press.
- 664 Dinstein, I., Thomas, C., Behrmann, M., & Heeger, D. J. (2008). A mirror up to nature. *Curr Biol*,
665 18(1), R13-R18.
- 666 Duda, R. O., Hart, P. E., & Stork, D. G. (2001). *Pattern classification*. *Int J Computational*
667 *Intelligence and Applications*, 1, 335-339.
- 668 Etzel, J. A., Zacks, J. M., & Braver, T. S. (2013). Searchlight analysis: promise, pitfalls, and
669 potential. *Neuroimage*, 78, 261-269.

- 670 Fabbri, S., Strnad, L., Caramazza, A., & Lingnau, A. (2014). Overlapping representations for grip
671 type and reach direction. *Neuroimage*, 94, 138-146.
- 672 Fabbri, S., Stubbs, K. M., Cusack, R., & Culham, J. C. (2016). Disentangling representations of
673 object and grasp properties in the human brain. *J Neurosci*, 36(29), 7648-7662.
- 674 Fang, F., & He, S. (2005). Cortical responses to invisible objects in the human dorsal and ventral
675 pathways. *Nat Neurosci*, 8(10), 1380-1385.
- 676 Fernández-Espejo, D., Rossit, S., & Owen, A. M. (2015). A thalamocortical mechanism for the
677 absence of overt motor behavior in covertly aware patients. *JAMA neurology*, 72(12),
678 1442-1450.
- 679 Fischer, J., Mikhael, J. G., Tenenbaum, J. B., & Kanwisher, N. (2016). Functional neuroanatomy
680 of intuitive physical inference. *Proc Natl Acad Sci USA*, 113(34), E5072-E5081.
- 681 Frey, S. H. (2007). What puts the how in where? Tool use and the divided visual streams
682 hypothesis. *Cortex*, 43(3), 368-375.
- 683 Frey, S. H. (2008). Tool use, communicative gesture and cerebral asymmetries in the modern
684 human brain. *Philos Trans R Soc Lond B Biol Sci*, 363(1499), 1951-1957.
- 685 Gallivan, J. P., Cant, J. S., Goodale, M. A., & Flanagan, J. R. (2014). Representation of object
686 weight in human ventral visual cortex. *Curr Biol*, 24(16), 1866-1873.
- 687 Gallivan, J. P., Cavina-Pratesi, C., & Culham, J. C. (2009). Is that within reach? fMRI reveals that
688 the human superior parieto-occipital cortex encodes objects reachable by the hand. *J*
689 *Neurosci*, 29(14), 4381-4391.
- 690 Gallivan, J. P., & Culham, J. C. (2015). Neural coding within human brain areas involved in
691 actions. *Curr Opin Neurobiol*, 33, 141-149.
- 692 Gallivan, J. P., Johnsrude, I. S., & Randall Flanagan, J. (2016). Planning ahead: object-directed
693 sequential actions decoded from human frontoparietal and occipitotemporal networks.
694 *Cerebral Cortex*, 26(2), 708-730.
- 695 Gallivan, J. P., McLean, D. A., Valyear, K. F., & Culham, J. C. (2013). Decoding the neural
696 mechanisms of human tool use. *Elife*, 2, e00425.
- 697 Gibson J. J. (1979) *The ecological approach to visual perception*. Boston: Houghton Mifflin.

- 698 Grafton, S. T., Fadiga, L., Arbib, M. A., & Rizzolatti, G. (1997). Premotor cortex activation during
699 observation and naming of familiar tools. *Neuroimage*, 6(4), 231-236.
- 700 Grèzes, J., Tucker, M., Armony, J., Ellis, R., & Passingham, R. E. (2003). Objects automatically
701 potentiate action: an fMRI study of implicit processing. *Eur J Neurosci*, 17(12), 2735-
702 2740.
- 703 Grill-Spector, K., Kourtzi, Z., & Kanwisher, N. (2001). The lateral occipital complex and its role in
704 object recognition. *Vision Research*, 41(10-11), 1409-1422.
- 705 Grill-Spector, K., Kushnir, T., Edelman, S., Avidan, G., Itzchak, Y., & Malach, R. (1999).
706 Differential processing of objects under various viewing conditions in the human lateral
707 occipital complex. *Neuron*, 24(1), 187-203.
- 708 Hutchison, R. M., Culham, J. C., Everling, S., Flanagan, J. R., & Gallivan, J. P. (2014). Distinct
709 and distributed functional connectivity patterns across cortex reflect the domain-specific
710 constraints of object, face, scene, body, and tool category-selective modules in the
711 ventral visual pathway. *Neuroimage*, 96, 216-236.
- 712 Imamizu, H., Kuroda, T., Miyauchi, S., Yoshioka, T., & Kawato, M. (2003). Modular organization
713 of internal models of tools in the human cerebellum. *Proc Natl Acad Sci USA*, 100(9),
714 5461-5466.
- 715 Ishibashi, R., Pobric, G., Saito, S., & Lambon Ralph, M. A. (2016). The neural network for tool-
716 related cognition: an activation likelihood estimation meta-analysis of 70 neuroimaging
717 contrasts. *Cogn Neuropsychol*, 33(3-4), 241-256.
- 718 Jacobs, S., Danielmeier, C., & Frey, S. H. (2010). Human anterior intraparietal and ventral
719 premotor cortices support representations of grasping with the hand or a novel tool. *J*
720 *Cogn Neurosci*, 22(11), 2594-2608.
- 721 Jarosz, A. F., & Wiley, J. (2014). What are the odds? A practical guide to computing and
722 reporting Bayes factors. *J Probl Solving*, 7(1), 2.
- 723 Johnson-Frey, S. H., et al., (2003). Actions or hand-object interactions? Human inferior frontal
724 cortex and action observation. *Neuron*, 39(6), 1053-1058.
- 725 Kanwisher, N. (2010). Functional specificity in the human brain: a window into the functional
726 architecture of the mind. *Proc Natl Acad Sci USA*, 107(25), 11163-11170.

- 727 Kay, K. N., Naselaris, T., Prenger, R. J., & Gallant, J. L. (2008). Identifying natural images from
728 human brain activity. *Nature*, 452(7185), 352-355.
- 729 Konkle, T., & Caramazza, A. (2013). Tripartite organization of the ventral stream by animacy and
730 object size. *J Neurosci*, 33(25), 10235-10242.
- 731 Kriegeskorte, N., Goebel, R., & Bandettini, P. (2006). Information-based functional brain
732 mapping. *Proc Natl Acad Sci USA*, 103(10), 3863-3868.
- 733 Lewis, J. W. (2006). Cortical networks related to human use of tools. *The neuroscientist*, 12(3),
734 211-231.
- 735 Lingnau, A., & Downing, P. E. (2015). The lateral occipitotemporal cortex in action. *Trends Cogn
736 Sci*, 19(5), 268-277.
- 737 Mahon, B. Z., & Caramazza, A. (2009). Concepts and categories: a cognitive neuropsychological
738 perspective. *Annu Rev Psychol*, 60, 27-51.
- 739 Mahon, B. Z., Milleville, S. C., Negri, G. A., Rumiat, R. I., Caramazza, A., & Martin, A. (2007).
740 Action-related properties shape object representations in the ventral stream. *Neuron*,
741 55(3), 507-520.
- 742 Maimon Mor, R. O., & Makin, T. R. (2020). Is an artificial limb embodied as a hand? *Brain
743 decoding in prosthetic limb users. PLoS Biol*, 18(6), e3000729.
- 744 Malach, R., Reppas, J. B., Benson, R. R., Kwong, K. K., Jiang, H., et al. (1995). Object-related
745 activity revealed by functional magnetic resonance imaging in human occipital cortex.
746 *Proc Natl Acad Sci USA*, 92(18), 8135-8139.
- 747 Maravita, A., & Iriki, A. (2004). Tools for the body (schema). *Trends Cogn Sci*, 8(2), 79-86.
- 748 Martin, A. (2007). The representation of object concepts in the brain. *Annu. Rev. Psychol.*, 58,
749 25-45.
- 750 Martin, A. (2016). GRAPES—Grounding representations in action, perception, and emotion
751 systems: How object properties and categories are represented in the human brain.
752 *Psychon Bull Rev*, 23(4), 979-990.
- 753 Martin, A., & Chao, L. L. (2001). Semantic memory and the brain: structure and processes. *Curr
754 Opin Neurobiol*, 11(2), 194-201.

- 755 Martin, A., Wiggs, C. L., Ungerleider, L. G., & Haxby, J. V. (1996). Neural correlates of category-
756 specific knowledge. *Nature*, 379(6566), 649-652.
- 757 Mizelle, J. C., Kelly, R. L., & Wheaton, L. A. (2013). Ventral encoding of functional affordances: a
758 neural pathway for identifying errors in action. *Brain and cognition*, 82(3), 274-282.
- 759 Monaco, S., Malfatti, G., Culham, J. C., Cattaneo, L., & Turella, L. (2020). Decoding motor
760 imagery and action planning in the early visual cortex: overlapping but distinct neural
761 mechanisms. *NeuroImage*, 116981.
- 762 Monaco, S., Sedda, A., Cavina-Pratesi, C., & Culham, J. C. (2015). Neural correlates of object
763 size and object location during grasping actions. *European J Neurosci*, 41(4), 454-465.
- 764 Mur, M., Bandettini, P. A., & Kriegeskorte, N. (2009). Revealing representational content with
765 pattern-information fMRI—an introductory guide. *Soc Cogn Affect Neurosci*, 4(1), 101-
766 109.
- 767 Oldfield, R.C. (1971). The assessment and analysis of handedness: The Edinburgh inventory.
768 *Neuropsychologia*, 9(1), 97-113.
- 769 Palser, E., & Cavina-Pratesi, C. (2018). Left lateral occipito-temporal cortex encodes
770 compatibility between hands and tools: an fMRI adaptation study. [10.31234/osf.io/kbjw4](https://doi.org/10.31234/osf.io/kbjw4)
771 (15 June 2019).
- 772 Peelen, M. V., & Downing, P. E. (2005). Is the extrastriate body area involved in motor actions?
773 *Nat Neurosci*, 8(2), 125-125.
- 774 Peelen, M. V., et al., (2013). Tool selectivity in left occipitotemporal cortex develops without
775 vision. *J Cogn Neurosci*, 25(8), 1225-1234.
- 776 Peeters, R. R., Rizzolatti, G., & Orban, G. A. (2013). Functional properties of the left parietal tool
777 use region. *Neuroimage*, 78, 83-93.
- 778 Perini, F., Caramazza, A., & Peelen, M. V. (2014). Left occipitotemporal cortex contributes to the
779 discrimination of tool-associated hand actions: fMRI and TMS evidence. *Front Hum*
780 *Neurosci*, 591.
- 781 Przybylski, Ł., & Króliczak, G. (2017). Planning functional grasps of simple tools invokes the
782 handindependent praxis representation network: an fMRI study. *J Int Neuropsychol Soc*,
783 23(2), 108-120.

- 784 Randerath, J., Goldenberg, G., Spijkers, W., Li, Y., & Hermsdörfer, J. (2010). Different left brain
785 regions are essential for grasping a tool compared with its subsequent use. *Neuroimage*,
786 53(1), 171-180.
- 787 Randerath, J., Goldenberg, G., Spijkers, W., Li, Y., & Hermsdörfer, J. (2011). From pantomime to
788 actual use: how affordances can facilitate actual tool-use. *Neuropsychologia*, 49(9),
789 2410-2416.
- 790 Rossit, S., McAdam, T., Mclean, D. A., Goodale, M. A., & Culham, J. C. (2013). fMRI reveals a
791 lower visual field preference for hand actions in human superior parieto-occipital cortex
792 (SPOC) and precuneus. *Cortex*, 49(9), 2525-2541.
- 793 Rouder, J. N., Morey, R. D., Speckman, P. L., & Province, J. M. (2012). Default Bayes factors for
794 ANOVA designs. *J Math Psychol*, 56(5), 356-374.
- 795 Rouder, J. N., Speckman, P. L., Sun, D., Morey, R. D., & Iverson, G. (2009). Bayesian t tests for
796 accepting and rejecting the null hypothesis. *Psychon Bull Rev*, 16(2), 225-237.
- 797 Sakuraba, S., Sakai, S., Yamanaka, M., Yokosawa, K., & Hirayama, K. (2012). Does the human
798 dorsal stream really process a category for tools? *J. Neurosci.* 32, 3949–3953.
- 799 Santello, M., Flanders, M., & Soechting, J. F. (1998). Postural hand synergies for tool use. *J*
800 *Neurosci*, 18(23), 10105-10115.
- 801 Singhal, A., Monaco, S., Kaufman, L. D., & Culham, J. C. (2013). Human fMRI reveals that
802 delayed action re-recruits visual perception. *PLoS One*, 8(9), e73629
- 803 Smith, F. W., & Muckli, L. (2010). Nonstimulated early visual areas carry information about
804 surrounding context. *Proc Natl Acad Sci USA*, 107(46), 20099-20103.
- 805 Smith, F.W. & Goodale, M.A. (2015). Decoding visual object categories in early somatosensory
806 cortex. *Cereb Cortex*, 25(4), 1020-1031.
- 807 Snow, J. C., et al., (2011). Bringing the real world into the fMRI scanner: Repetition effects for
808 pictures vs real objects. *Sci Rep*, 1, 130.
- 809 Striem-Amit, E., Vannuscorps, G., & Caramazza, A. (2017). Sensorimotor-independent
810 development of hands and tools selectivity in the visual cortex. *Proc Natl Acad Sci USA*,
811 114(18), 4787-4792.

- 812 Styrkowiec, P. P., Nowik, A. M., & Króliczak, G. (2019). The neural underpinnings of haptically
813 guided functional grasping of tools: an fMRI study. *Neuroimage*, 194, 149-162.
- 814 Talairach, J. & Tournoux, P. (1988). *Co-Planar Stereotaxic Atlas of the Human Brain*. Thieme,
815 New York.
- 816 Umiltà, M. A., Intskirveli, I., Grammont, F., Rochat, M., Caruana, F., Jezzini, A., Gallese, V., &
817 Rizzolatti, G. (2008). When pliers become fingers in the monkey motor system. *Proc Natl*
818 *Acad Sci USA*, 105(6), 2209-2213.
- 819 Valyear, K. F., Cavina-Pratesi, C., Stiglick, A. J., & Culham, J. C. (2007). Does tool-related fMRI
820 activity within the intraparietal sulcus reflect the plan to grasp? *Neuroimage*, 36, 94-108.
- 821 Valyear, K. F., & Culham, J. C. (2010). Observing learned object-specific functional grasps
822 preferentially activates the ventral stream. *J Cogn Neurosci*, 22(5), 970-984.
- 823 Valyear, K. F., Fitzpatrick, A. M., & McManus, E. F. (2017). "The neuroscience of human tool
824 use" in *Evolution of Nervous Systems*. Kaas, J. (Ed.), pp. 341-353, Elsevier, Oxford.
- 825 Valyear, K. F., Gallivan, J. P., McLean, D. A., & Culham, J. C. (2012). fMRI repetition
826 suppression for familiar but not arbitrary actions with tools. *J Neurosci*, 32(12), 4247-
827 4259.
- 828 Van den Heiligenberg, F. M., et al., (2018). Artificial limb representation in amputees. *Brain*,
829 141(5), 1422-1433.
- 830 Wagenmakers, E. J. (2007). A practical solution to the pervasive problems of p values. *Psychon*
831 *Bull Rev*, 14(5), 779-804.
- 832 Weisberg, J., Van Turenout, M., & Martin, A. (2007). A neural system for learning about object
833 function. *Cereb Cortex*, 17(3), 513-521.
- 834 Yoon, E. Y., Humphreys, G. W., Kumar, S., & Rotshtein, P. (2012). The neural selection and
835 integration of actions and objects: an fMRI study. *J Cogn Neurosci*, 24(11), 2268-2279.

836 **Figure Legends**

837 **Figure 1.** Experimental set-up and design. (A) 3D-printed tool and non-tool control object pairs
838 (black markers on objects indicate grasp points) which were matched for elongation, width and
839 depth such that tool and non-tool actions were biomechanically similar. (B) Side view of real
840 action participant set-up used to present 3D objects at grasping distance (without the use of
841 mirrors). Red star indicates fixation LED. The hand is shown at its starting position. (C) Timing
842 and grasping tasks from subject's point of view for the real action experiment. During the 10s
843 ON-block the object was illuminated 5 times cueing the participant to grasp the object each time
844 by its left or right side (as per preceding auditory cue) with the right hand. Exemplar videos of trial
845 types can be accessed here: <https://osf.io/gsmyw/>. This was followed by a 10s OFF-block
846 involving no stimulation where the workspace remained dark. For MVPA, we treated tool and
847 non-tool trials independently, where for the tools only, right- and left-sided grasps were typical
848 and atypical grasps respectively (based on handle orientation). (D) Timing of visual localizer
849 experiment. In the visual localizer, blocks of tools, hands, chairs, bodies and scrambled 2D
850 image stimuli were presented in between fixation-only screens. (E) For each individual participant
851 independent ROIs were defined for MVPA using functional activity from the visual localizer
852 (Table 1). The representative ROI locations are displayed on a group activation contrast map
853 from the visual localizer (All conditions > (Baseline*5)) projected onto a left hemisphere cortical
854 surface reconstruction of a reference brain (COLIN27 Talairach) available from the neuroElf
855 package (<http://neuroelf.net>).

856

857 **Figure 2.** Grasp type decoding results in left hemisphere ROIs. (A) Violin plots of MVPA data
858 from visual localizer ROIs for the typical vs atypical classification of grasping tools (white violins)
859 and, non-tool control grasping (right vs left decoding; grey violins). Box plot centre lines are mean
860 decoding accuracy while their edges and whiskers show ± 1 SD and ± 2 SEM, respectively.
861 Decoding accuracies of typical vs atypical grasping in IPS and LOTC hand-selective cortex (pink)
862 are significantly greater-than-chance for tools, but not non-tools. (B) ANOVA results comparing
863 the difference of decoding accuracy between tools (typical vs atypical) and non-tools (right vs
864 left) for the partially overlapping hand- and tool-selective ROIs within the IPS and LOTC. (C)

865 Violin plot of MVPA data for control ROI in somatosensory cortex (SC) based on an independent
866 contrast (all actions > baseline) from real action experiment showing significant decoding of
867 grasp type for both tools and non-tools. Red asterisks show FDR-corrected results while black
868 asterisks show uncorrected results.

869

870 **Figure 3.** Grip size decoding. (A) We decoded smaller vs larger objects in three separate
871 decoding analysis, regardless of whether the objects were tools or non-tools. Each separate grip
872 size pair decoding analysis is shown in each row of images of Fig.3A (from top to bottom: small
873 vs. medium; small vs. large; medium vs. large). The heads of the knife, spoon and pizzacutter
874 tools and their paired non-tools had matched small, medium and large widths, respectively.
875 Decoding accuracies for each grip size pair were then averaged and tested against chance using
876 a one-tailed one-sample t-test. In all cases, object category was collapsed to maximise power
877 and generalisability (i.e., grasping tools and non-tools), and reach direction was matched to
878 minimise kinematic variance (i.e., all actions were leftward). (B) Mean decoding accuracy in
879 visual localizer ROIs for the small versus large classification collapsed across object category.
880 Error bars represent ± 1 SEM.

881

882 **Figure 4.** Mean activation (β) per ROI and condition used as input for pattern classification and
883 univariate analyses. Error bars represent ± 1 SEM.

884

885

886

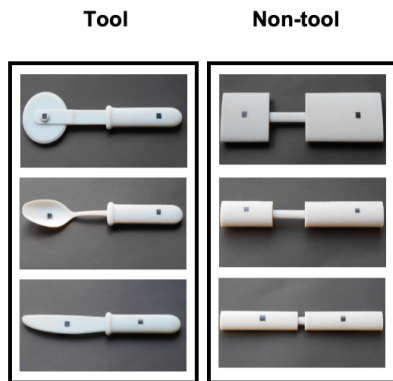
887

888 **Table 1.** Visual Localizer ROI descriptives. ROI subject counts with their mean sizes (voxels) and
 889 peak coordinates (Talairach).

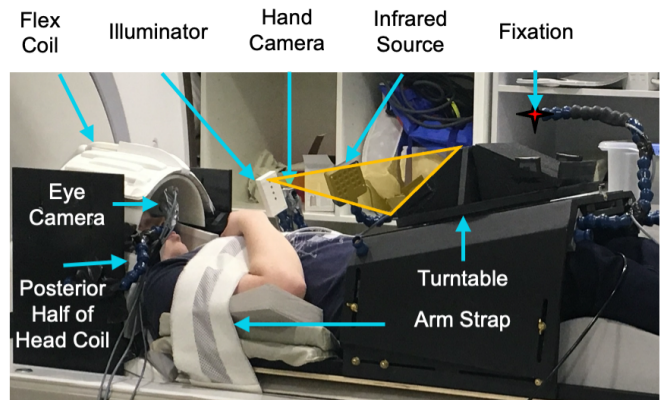
ROI	N Subjects with ROI	Mean size (SD)	Mean peak coordinates (SD)		
			X	Y	Z
EVC	19	114 (35)	-14 (6)	-89 (4)	-9 (9)
LOTG-Object	19	148 (34)	-42(4)	-77 (4)	-7 (4)
LOTG-Body	18	55 (30)	-45 (3)	-76 (5)	2 (6)
LOTG-Hand	17	81 (44)	-47 (4)	-71 (4)	-1 (5)
LOTG-Tool	17	77 (45)	-47 (5)	-71 (5)	-2 (6)
pMTG	17	96(48)	-45 (4)	-57 (3)	3 (4)
pFs	19	105 (41)	-40 (4)	-54 (4)	-14 (4)
SMG	17	69 (43)	-53 (6)	-28 (4)	27 (6)
IPS-Hand	19	110 (57)	-38 (4)	-46 (7)	42 (3)
IPS-Tool	19	81 (55)	-37 (5)	-41 (7)	42 (5)
PMv	14	61 (42)	-45 (7)	-1 (6)	31 (5)
PMd	14	47 (28)	-29 (5)	-13 (4)	51 (4)

890

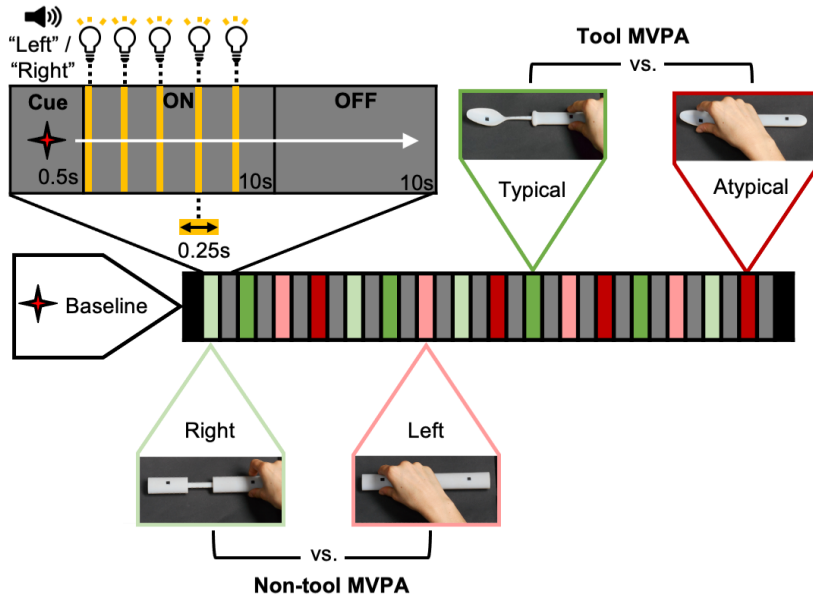
A 3D-Printed Stimuli



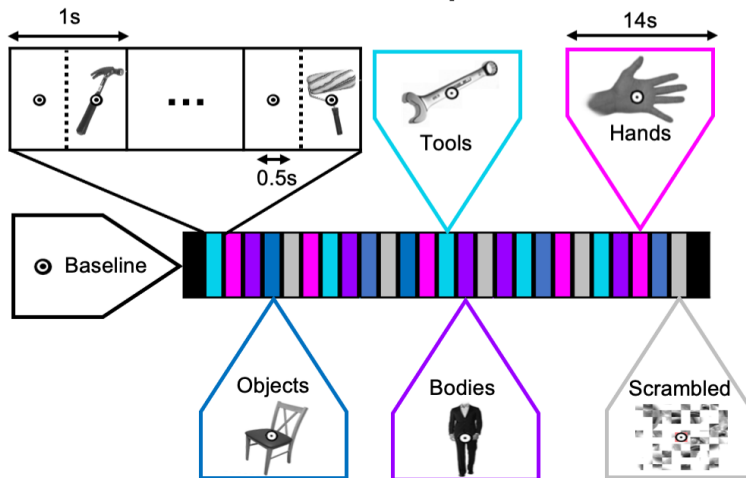
B Real Action fMRI Setup



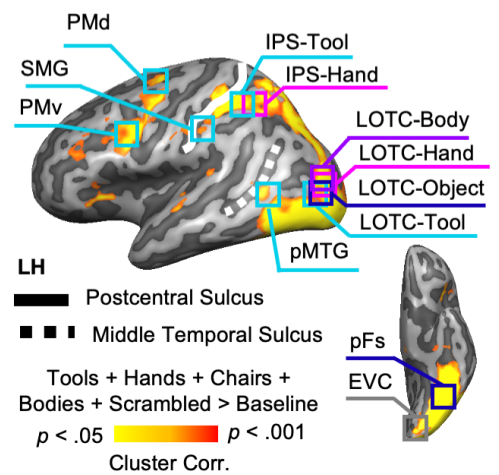
C Real Action Experiment

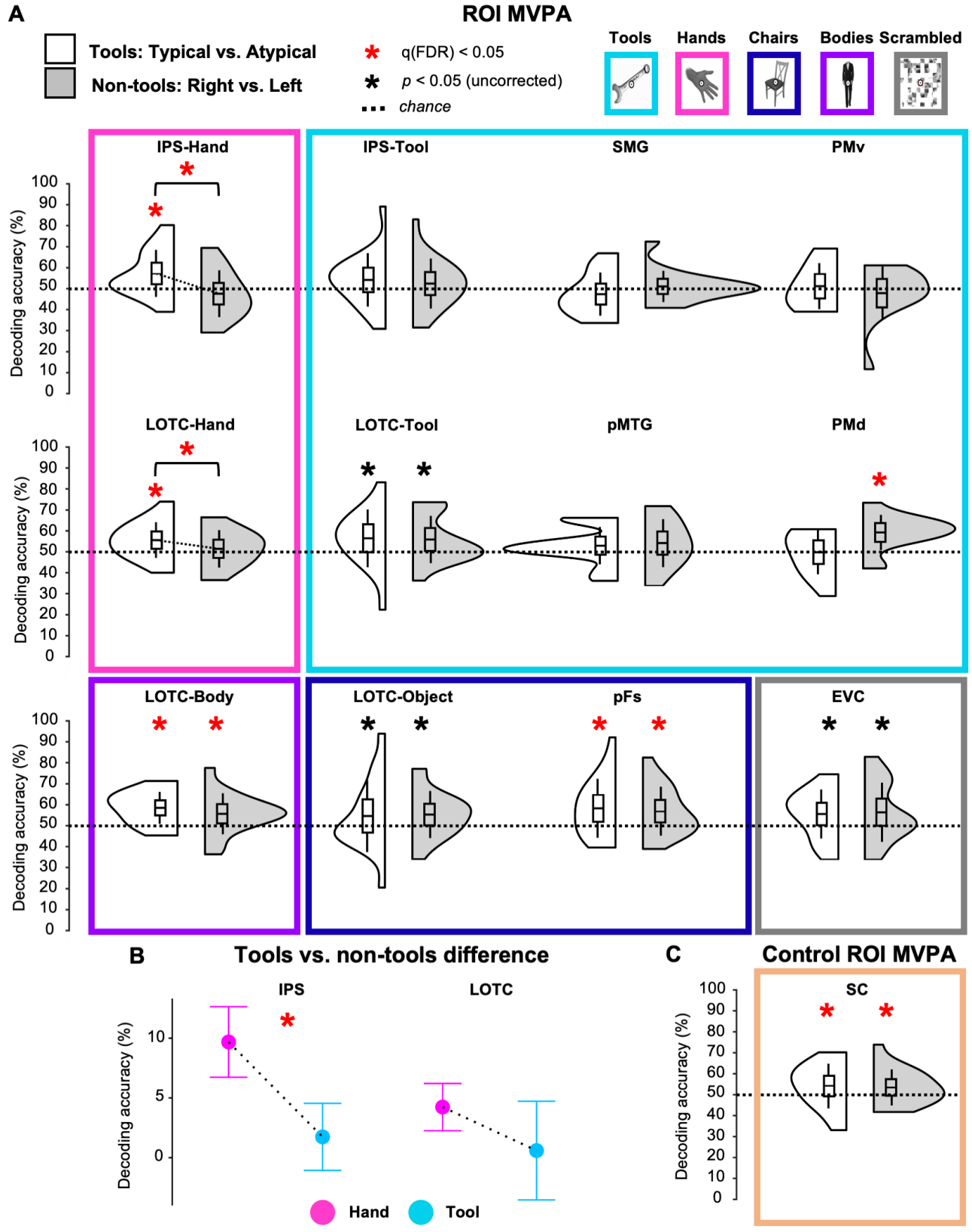


D Visual Localizer Experiment

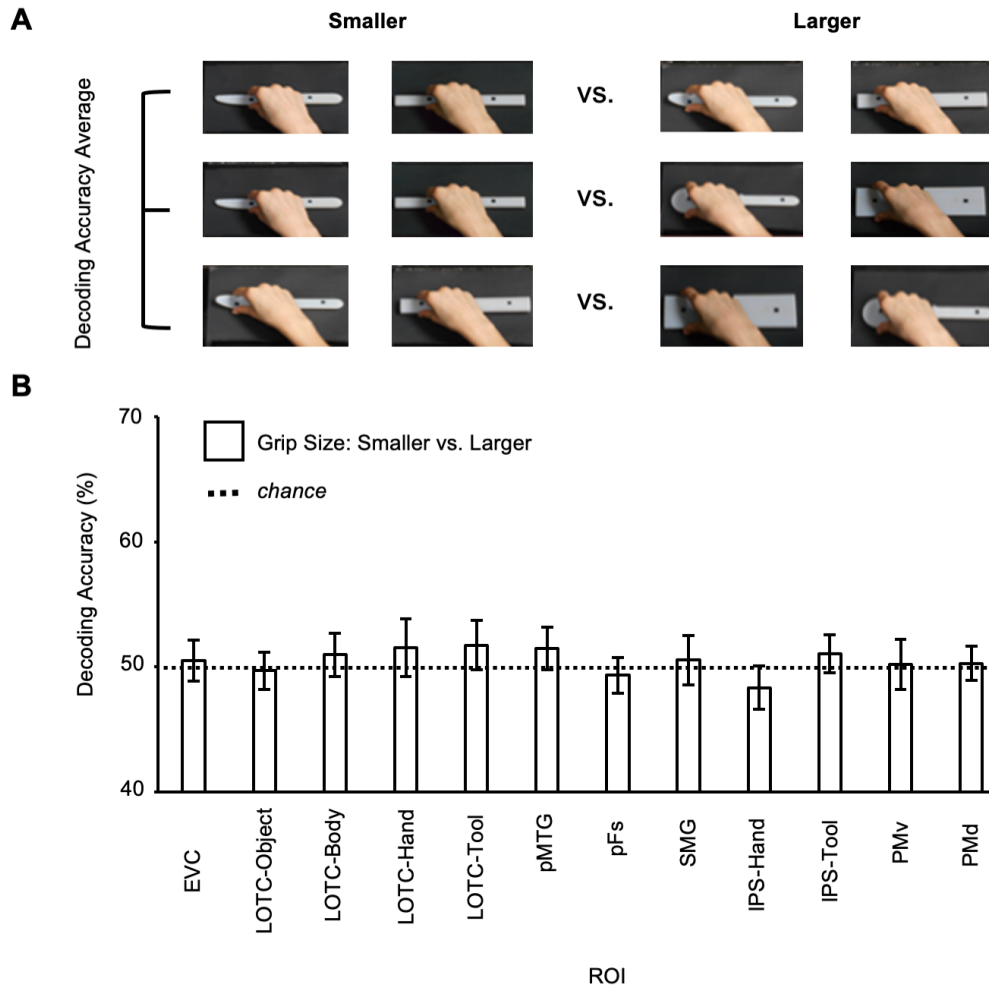


E Localizer ROIs





Grip Size Control MVPA



ROI Univariate Analysis

